Shahrood University of Technology
Iranian Society of Mining Engineering (IRSME)
Journal of Mining and Environment (JME)
journal homepage: www.jme.shahroodut.ac.ir
THOMSON REUTERS

An Investigation on Tailing Slurry Transport in Kooshk lead-Zinc Mine in Iran Based on Non-Newtonian Fluid Rheology: an Experimental Study

Javad Vazifeh Mehrabani[1*] and Mohammad Goharkhah [2]

1- Department of Mineral Processing, Faculty of Mining Engineering, Sahand University of Technology, Sahand New Town, Tabriz, Iran
2- Faculty of Mechanical Engineering, Sahand University of Technology, Sahand New Town, Tabriz, Iran

Article Info

Received 24 August 2021
Received in Revised form 18 September 2021
Accepted 24 September 2021
Published online 24 September 2021

DOI:10.22044/jme.2021.11105.2093

Keywords

Tailing slurry
Critical velocity
Pipe design
Bingham model
Kooshk mine

Abstract

In the current research work, a piping system is designed for slurry transport to the tailing dam in the Kooshk lead-zinc mine, Iran. The experiments are carried out primarily to investigate the rheological behavior of the slurry at different densities and obtain a non-Newtonian model for the shear stress variation with the deformation rate. It is shown that the shear stress of concentrated slurry follows the plastic Bingham model. The results obtained also indicate the increasing trend of the yield stress and the apparent viscosity of the slurry with the density. Appropriate correlations are proposed for the apparent viscosity and yield stress as a function of pulp concentration. At the next step, the required design parameters such as the slurry flow rate, pressure drop, critical velocity, and minimum required head for flow initiation and head losses are calculated for different slurry densities and pipe sizes. The appropriate piping system is finally designed based on the experimental data and the calculated parameters. It is concluded that the 3 in diameter pipe can be used to deliver the slurry with solid concentrations between 44% < Cw < 60% by weight, without a pumping system.

1. Introduction

Slurry is a concentrated mixture of solid particles with a carrier liquid. Slurry transport by pipelines is widespread in various industries such as minerals, chemical, food, and water owing to energy efficiency, environment friendliness, and simple control advantages [1, 2]. Slurry flow in pipes is hydro-dynamically different from single-phase liquid flows. For single-phase flows, an extensive range of velocities is possible in the pipes, and a flow regime is determined according to the fluid and system properties. To the contrary, involvement of the two different flow regimes of homogeneous and heterogeneous slurries accompanied with additional fluid properties adds to the complexity of the slurry transport problem. In the homogeneous mixtures, fine particles are uniformly distributed in the carrier liquid, and the solid particle volume fraction in generally high. Such slurries exhibit a non-Newtonian behavior, and thus the inertial effects do not exert a major influence on the bulk velocity. On the other hand, cross-sectional concentration gradients exist in the heterogeneous slurries. These slurries have lower particle concentrations, and contain larger particle sizes than the homogeneous slurries [3-6]. The slurries encountered in the industrial applications are generally of mixed characteristic, i.e. the fine particles form a homogeneous mixture and the coarse particles form a heterogeneous mixture with the carrier fluid. Determination of the characteristics of the slurry based on the slurry type is thus an important issue in the design of a slurry transport system [6]. To this end, several parameters that have crucial roles on the slurry system are required to be taken into account. The critical velocity, particle size and concentration, rheology of the slurry, pressure drop, velocity distribution, and friction losses are among the most

Corresponding author: mehrabani@sut.ac.ir (J. Vazifeh Mehrabani).

important parameters for an efficient design of a slurry transport system.

In order to achieve a stable operation of a pipeline, the bulk slurry velocity must be equal to or greater than a particular value called the critical velocity [3, 7]. One of the first correlations of the critical velocity that has been widely used has been proposed by Durand [8] based on the experimental data. Several correlations have also been developed during the past few decades [9-14]. The models developed by Wilson and Judge [9], and by Thomas [10], are based on both the theoretical and experimental concepts, and their applications cover a broad range of fluid properties and pipe diameters. The model developed by Wasp et al. [3] takes into account the particle size distribution in the transport process. Wasp and Slatter [11] have proposed a critical velocity model as a function of the system variables including the pipe diameter, volume concentration, particle size and density, and slurry viscosity. The model of Doron and Barena [12] is a three-layer model based on a mechanical balance. Lahiri and Ghanta [13] have derived their model by employing artificial intelligence to fit the experimental data. A comprehensive review of the previous models has been carried out by Gillies et al. [14].

The slurry concentration and particle size distribution in the pipelines are other parameters that have been focused on in a number of studies [16-21]. Miedema [16] has developed methods for calculation of the radial distribution of the particle concentration based on the eddy diffusivity and particle settling velocity. Kaushal and Tomita [17] have carried out experiments on a heterogeneous slurry, observing that the maximum value of the particle concentration occurs at the distance of 0.2D from the pipe surface. It was attributed to the near wall lift effect on the solid particles [18]. Tarodiya and Ganndhi [19] have studied the effect of particle size distribution on the performance of a centrifugal slurry pump handling multi-size particulate slurry. Reduction in the intensity of granular pressure, maximum granular viscosity, and the head loss due to friction in impeller and casing flow passages were observed with the increase in the particles size. Knezevic and Kolonja [20] have indicated the influence of particle distribution on the pressure drop of ash slurries through pipeline transportation.

Slurries exhibit a Newtonian or non-Newtonian behavior according to the particle volume fraction. Rheology of slurries is thus an important parameter that has been investigated previously [22–27]. Senapati and Mishra [24] have developed a non-Newtonian pseudo-plastic power law head loss model in order to predict the pressure drop of ash slurries through pipeline transportation. Xiao et at. [25] have experimentally examined the rheological properties of slag-cemented paste backfill, indicating that the yield stress and viscosity of the slurry increase over the curing time. Verma et al. [26] have investigated the rheological behavior of highly concentrated fly ash slurries. Their results showed that the Bingham plastic model could be used for modeling of the slurry viscosity. Moreover, the yield shear stress and apparent viscosity were obtained through experiments. Cao et al. [27] have carried out experiments on the rheological and sedimentation characteristics of fresh cemented tailings, developing functions for variations in the shear stress, viscosity, and sedimentation rate.

The flow characteristics of slurry in the piping systems such as pressure drop, velocity distribution, and friction losses have also been studied by several researchers [28-31]. Miedema [28] has developed a slip velocity and a head loss model for slurry transport in the heterogeneous regime. In contrast to the previous models, his model consists of two terms for the excess pressure losses including kinetic energy and potential energy losses. Wu et al. [29] have numerically and experimentally investigated the pressure drop in a loop pipe flow of fresh cemented coal gangue–fly ash slurry. The effects of slurry volumetric flow rate and pumping pressure as well as the combined effect of pipe inner diameter and flow velocity on pressure drop in the pipe loop flow of slurry were demonstrated. Kumar et al. [30] have investigated the effect of particle gradation on pressure drop of ash slurries in the pipeline, proposing a model to predict the pressure drop and solid distribution of the slurries. Comparison of the numerical results and the experimental data in the studies of this category has revealed that there is a significant discrepancy in the concentration profile especially near the pipe surface. It should be noted that slurries in the real operational conditions contain particles with different sizes. This is generally neglected in the numerical simulations, and leads to a significant difference between the numerical and experimental results [31].

The above-mentioned key parameters have been employed in a number of research works in order to simulate as well as design efficient slurry transport systems. Ling et al. [32] have numerically investigated the liquid–solid slurry flows in a fully developed turbulent flow. Li et al. [33] have studied the minimum specific energy consumption

and optimal transport concentration of the slurry pipeline transport systems. The influence of several parameters such as the particle-gradation uniformity coefficient, median particle size, pipe diameter, and particle volume concentration were analyzed. Their results obtained revealed that the greater the uniformity coefficient, the smaller the minimum specific energy consumption and the larger the optimal transport concentration for a constant, median particle size slurry. Ihle [34] has introduced the concept of optimal diameter for settling slurries, proposing a simple model to assess the most economic pipeline diameter based on several aspects such as the deposit velocity, energy and water costs, and pipe infrastructure cost. Cunliffe [35] has developed a simple framework to enable the accurate prediction of the bulk flow behavior and settling characteristics of slurries in open conduits, and has validated it experimentally. He investigated the effects of different parameters including the flow rate, flow depth and settling regime, solid concentration, Reynolds number, and Froude number. His proposed method can be used to make primary predictions of critical sedimentation velocities to minimize the environmental and commercial costs of slurry transport.

In the current work, a piping system is designed for tailing slurry transport in the Kooshk lead-zinc mine in Iran. The piping system is desired to transport the pulp with a maximum possible solid concentration by weight.

As mentioned earlier, several parameters have crucial roles on the slurry system. Determination of the characteristics of the slurry is thus an important issue in the design of a slurry transport system. The rheological behavior of the pulp has a significant impact on the design of a slurry piping system. Thus it is necessary to primarily investigate the rheological behavior of the pulp, and develop an appropriate model. In this work, at the first step, an experimental study is carried out in order to identify the tailing pulp behavior. Then the required parameters such as the friction head losses and the pressure drop values are calculated at different pulp concentrations and pipe sizes. Finally, the appropriate piping system is designed based on the experimental data, developed models, and numerical calculations.

The paper structure is as what follows. In Section 2, the Kooshk lead-zinc mine as the studied case is introduced. In Section 3, the experimental procedure and main test issues are explained. Section 4 summarizes the formulation and the governing equations. The properties of the pulp are given in Section 5. Section 6 presents the results including the validation of the experiments, obtained data, and developed models. An economical evaluation of the piping system is presented in Section 7. Final remarks are given in the conclusion section.

2. Problem description

The Kooshk lead−zinc mine located in the desert and semi-arid land of Bafgh, Yazd Province, is one of the main sulfide deposits in Iran. The final flotation tailing of the mineral processing plant including two streams of pre-flotation and scavenger tailings are combined and transported to the tailing thickener. The discharged tailing slurry from the thickener underflow is transported by gravity using an open channel. Due to the open channel geometry and gravity limitations, the tailing slurry is unfavorably transported with low solid content to the tailing dam, and water recovery from the thickener is thus inefficient. Considering the lack of water in the semi-arid region, a higher water recovery system from the tailing thickener is necessary form the environmental and economic viewpoints. A preliminarily evaluation indicated that replacement of the open channel with a pipe system could be an appropriate solution, and transportation of tailing slurry will be possible with a higher solid content, and consequently, a lower water loss. The slurry transport path from the thickener to the tailing dam is obtained from field observation data and satellite images, and is depicted in Figure 1.

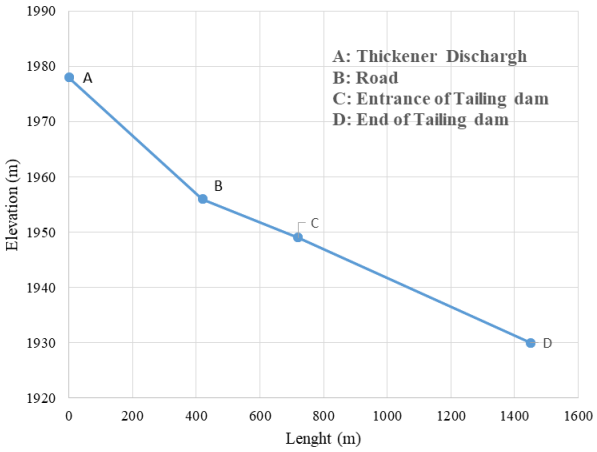

Figure 1. Tailing transport path from thickener discharge to tailing dam.

As shown in this figure, the current tailing transport path consists of two sections with different slopes; a path of 400 m length and 5% slope from the thickener underflow to the main

road and a path of about 1000 m length and 2% slope from the road to the end of the tailing dam. The dam is located 300 m far from the road. Transport of the pulp slurry is currently carried out in an open channel with concentration of solid in the range of 35-45% by weight. The low slope of the second section causes serious problems in the tailing transport in the open channel. Thus it is desired to replace the current open channel path with a closed piping system. The designing process of the piping system requires consideration of the wall shear stress distribution and pressure drop variation with pulp flow rate and pipe diameter. However, the conventional Newtonian fluid model cannot be applied for the pulp flow. The pulp slurry consists of coarse solid particles, and is anticipated to exhibit a non-Newtonian behavior. Thus it is necessary to primarily investigate the rheological behavior of the pulp and develop an appropriate model for the apparent viscosity. The main pressure drop calculations are then carried out using the developed models, and an appropriate piping system is recommended.

3. Experimental Procedure

3.1. Experimental setup

An experimental setup is designed and constructed to study the pulp rheological properties. A schematic representation of the setup is shown in Figure 2.

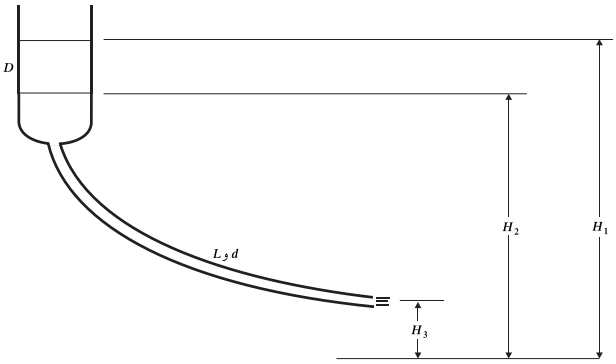

Figure 2. A schematic representation of the test section.

As shown in this figure, the setup consists of a cylindrical tank and a pipe connected to the bottom surface. The pulp surface inside the tank descends from the original level of H_1 to the final level of H_2, and discharges to the atmosphere at the elevation of H_3. The experiments are carried out for different tank and tube diameters, tube lengths, and pulp concentrations, and the exit flow rate Q is obtained as a function of the pulp level H in the tank. The H-Q data obtained is used to investigate the rheology of the pulp and develop a non-Newtonian model for the apparent viscosity of the pulp slurry. The obtained slurry viscosity is finally used to calculate the friction head losses at different operating conditions, and consequently, design the appropriate piping system.

3.2. Experimental and design considerations

There are a number of important points that are required to be taken into account during performing the experiments as well as designing the piping system. The change in the flow regime, flow developing length before a fully developed region, friction losses, accelerational term in the Bernoulli equation due to the transient flow, and flow stabilization time are discussed in the following sub-sections.

3.2.1. Dynamic similarity

For the experimental data to be extendable to the real situation, the dynamic similarity between the experimental setup and the original system is necessary. In other words, the Reynolds number must be equal for the test and original conditions in order to assure the dynamic similarity. Since the pulp flow is used in both cases, the product of velocity and pipe diameter (VD) is required to be kept constant for the test and real situations. This means that the velocity in the experiments must be ten times that of the original condition if the dimensions are scaled, for example, 1/10. The important point is that the velocity increase should not lead to the change in the flow regime from laminar to turbulent.

3.2.2. Developing length

The pipe length is required to be larger than the hydro-dynamic entrance length in order to perform the pressure drop calculations. This point has been taken into account in the selection of the pipe length in the current experiments.

3.2.3. Flow stabilization time

The unsteady fluid motion in a tube with length of L and diameter of D is governed by the following equation [36]:

$$\rho g\left(h_t - f\frac{L}{D}\frac{V^2}{2g}\right) = \rho L\frac{dV}{dt} \quad (1)$$

For a steady flow with velocity V_t, h_t is the head loss calculated from [36, 37]:

$$h_t = f\frac{L}{D}\frac{{V_t}^2}{2g} \quad (2)$$

where f is the friction factor. Eqs. 1 and 2 can be combined and integrated to obtain:

$$t = \frac{LV_t}{2gh_t}\ \ln\frac{V_t + V}{V_t - V} \quad (3)$$

Considering Eq. 3, the time required for flow velocity to reach $0.99V_t$ is defined as the flow stabilization time, and can be obtained as:

$$t = 2.65\frac{LV_t}{gh_t} \quad (4)$$

3.2.4. Critical velocity

The settling velocity is the rate at which a solid particle settles in a fluid. It is a function of particle size and shape, particle and fluid specific gravity, and fluid viscosity. On the other hand, the deposition critical velocity is the minimum required flow velocity to move the initially settled solid particles. Thus the flow velocity is required to be higher than the critical deposition velocity in any piping system [5]. For velocities lower than the critical velocity, decreasing the flow velocity increases the friction losses since it increases the particles deposition, while the friction loss increases with the flow velocity for velocities higher than the critical value. The deposition critical velocity depends on the settling velocity of the coarse solid particles, and it generally increases with the particle size, density, particles volume fraction, and viscosity [6]. A number of correlations are proposed for calculation of the critical velocity. The Durand correlation is written as [8]:

$$V_c = F_L\sqrt{2gD(S-1)} \quad (5)$$

where F_L is the settling velocity parameter, and depends on the particle size and concentration. A modified form of the Durand correlation is given as follows:

$$V_c = 1.25\ F_L 2gD(S-1)^{1/4} \quad (6)$$

where S is the specific gravity. Another correlation has been proposed by Wasp *et al*. [3], written as follows:

$$V_c = 3.116\ {C_v}^{0.186}\sqrt{2gD(S-1)}(\frac{d_{50}}{D})^{1/6} \quad (7)$$

The Cave and Elvin correlations were also proposed as [38]:

$$V_c = 1.04D^{0.3}(S-1)^{0.75}\ln\left(\frac{d_{50}}{16}\right)[\ln\left(\frac{60}{C_v}\right)]^{0.13} \quad (8)$$

Furthermore, the following correlation has been proposed by Schiller and Herbich [39]:

$$V_c = 1.3{C_v}^{0.125}[1-\exp(-6.9d_{50})]\sqrt{2gD(S-1)} \quad (9)$$

where C_v , D, and d are the concentration of solid by volume, pipe diameter, and particle diameter, respectively.

4. Shear stress, pressure drop, and head loss equations

4.1. Newtonian fluid

In the Newtonian fluids, the shear stress is a linear function of the deformation rate. In such fluids the flow velocity is high enough to suspend the solid particles [6]. The energy equation for a piping system as well as for the current experimental setup can be written as follows [36, 37]:

$$\frac{P_1}{\gamma} + \frac{V_1^2}{2g} + z_1 = \frac{P_2}{\gamma} + \frac{V_2^2}{2g} + z_2 + h_f + K\frac{V_2^2}{2g} \quad (10)$$

where the indices 1 and 2 refer to the fluid surface in the tank and at the pipe exit, respectively, h_f is the friction head loss, and K is the minor losses coefficient. h_f can be calculated using Eq. 2.
The average elevation head difference between the points 1 and 2 in Figure 1 is:

$$H = \frac{(H_1 + H_2)}{2} - H_3 \quad (11)$$

A steady and fully developed flow occurs due to the above-mentioned elevation differences. Eq.10 can be written for the laminar and turbulent flows, as given in the following sections.

4.1.1. Laminar flow

The friction factor f is a function of the Reynolds number for laminar flow, as follows [36]:

$$\mathrm{f} = \frac{64}{Re} \quad (12)$$

Assuming a negligible kinetic energy and connection losses at the pipe exit, the elevation head will be equal to the friction losses [36]. Thus:

$$H = \frac{128\mu LQ}{\pi\rho g d^4} = \frac{128\upsilon LQ}{\pi g d^4} \quad (13)$$

where Q is the flow rate. The kinematic viscosity υ can be obtained from [36, 37]:

$$\upsilon = \frac{\pi g d^4}{128L}\frac{H}{Q} \quad (14)$$

Furthermore, the pressure drop and wall shear stress in the laminar flow are obtained from the Hagen-Poiseuille equation [36, 37].

$$\Delta P = \frac{8\mu LQ}{\pi R^4} \quad (15)$$

$$\tau = \frac{\Delta PR}{2L} \quad (16)$$

4.1.2. Turbulent flow

Considering the mentioned assumptions for the laminar flow, the friction factor can be calculated from the following equation for the turbulent flow [36, 37]:

$$f = \frac{0.2}{Re^{0.2}} \quad (17)$$

The elevation head and the viscosity are also related, as follows:

$$H = \frac{0.1}{g}(\frac{4}{\pi})^{1.8}\nu^{0.2}\frac{L}{d^{4.8}}Q^{1.8} \quad (18)$$

4.1.3. Turbulent flow with kinetic energy and minor head losses

The energy equation in this case is simplified to [36, 37]:

$$H = (f\frac{L}{D} + K + 1)\frac{V^2}{2g} \quad (19)$$

$$f = \frac{d}{L}(\frac{2gH}{V^2} - K - 1) \quad (20)$$

4.2. Non-Newtonian fluid

4.2.1. Rheology of non-Newtonian fluid

For the colloidal micro-sized particles, the fluid deviates from the Newtonian behavior, and exhibits a non-Newtonian behavior. The shear stress is not a linear function of the shear rate for this type of fluids. Several models such as the pseudo-plastic, Bingham plastic, Herschel-Bulkley, and Casson models have been proposed for simulation of the non-Newtonian fluids [36, 37]. The plastic Bingham is an ideal fluid model that can be used for highly concentrated pulps with tiny particles. The shear stress in this model is expressed as:

$$\tau = \tau_o + \eta\dot{\gamma} \quad (21)$$

where τ_o is the yield stress, $\dot{\gamma}$ is the deformation rate, and k is a constant. The relation between the shear rate and the shear stress for a non-Newtonian fluid can be obtained by the Robinowitsch-Mooney equation, as follows [40]:

$$-\dot{\gamma} = \frac{8u}{d_i}[\frac{3}{4} + \frac{1}{4}\frac{dln\left(\frac{8u}{d_i}\right)}{dln(\tau_\omega)}] \quad (22)$$

Eq. 22 implies that the shear rate for a non-Newtonian fluid can be calculated from the value for a Newtonian fluid having the same flow rate in the same pipe multiplied by a correction factor. The correction factor consists of a derivative term. It is estimated by plotting the values of $\ln(\frac{8V}{d})$ against $\ln(\tau_w)$ obtained from the experiments. The former is obtained from the flow rate measurements, and the latter can be calculated from the elevation head values.

4.2.2. Pressure drop for non-Newtonian fluids

Two non-dimensional numbers are defined for non-Newtonian fluids as [40]:
Reynolds number:

$$\mathrm{Re} = \frac{\rho VD}{\eta} \quad (23)$$

Hedstrom number:

$$\mathrm{He} = \frac{\rho D^2\tau_o}{\eta^2} \quad (24)$$

where η is the apparent viscosity. The friction factor is calculated from Eqs. 25 and 26 for the laminar and turbulent flows, respectively [41].

$$f_L = \frac{64}{\mathrm{Re}}\left[1 + \frac{\mathrm{He}}{6\mathrm{Re}} - \frac{1}{3}\frac{\mathrm{He}^4}{f^3\mathrm{Re}^7}\right] \quad (25)$$

$$f_T = 4\times10^{-1.47\left[1+0.146e^{-2.9\times10^{-5}\mathrm{He}}\right]}\mathrm{Re}^{-0.193} \quad (26)$$

The laminar to turbulent flow transition occurs at the critical Reynolds number of $\mathrm{Re_c} = 2000$ for the Newtonian fluids. On the other hand, the critical Reynolds for the non-Newtonian fluids is estimated by the Hanks correlation [42], as follows:

$$\mathrm{Rec} = \frac{\mathrm{He}}{8\phi}\left(1 - \frac{4}{3}\phi = \frac{1}{3}\phi^4\right) \quad (27)$$

where ϕ is obtained from the following equation by the trial-and-error method.

$$\mathrm{He} = 16800\frac{\phi}{(1-\phi)^3} \quad (28)$$

Alternatively, the correlation proposed by Darby can be used for both the laminar and turbulent flows [43].

$$f = [f_L^m + f_T^m]^{1/m} \quad (29)$$

where:

$$m = 1.7 + \frac{40000}{\mathrm{Re}} \quad (30)$$

4.2.3. Pressure required for flow initiation

The plastic Bingham fluids require a minimum pressure or head to overcome the yield stress, and start to flow in the pipe. The minimum head is related to the yield stress, as follows [43]:

$$H_{st} = \frac{4\tau_o L}{\rho g D} \quad (31)$$

5. Pulp properties

The particle size distribution and concentration are important restrictions in pumping mixtures of solids and carrier fluids, and can impact on the flow stability and pipe surface wear. A sample of the tailing thickener is studied primarily. The cumulative passing as a function of the particle size is shown in Figure 3.

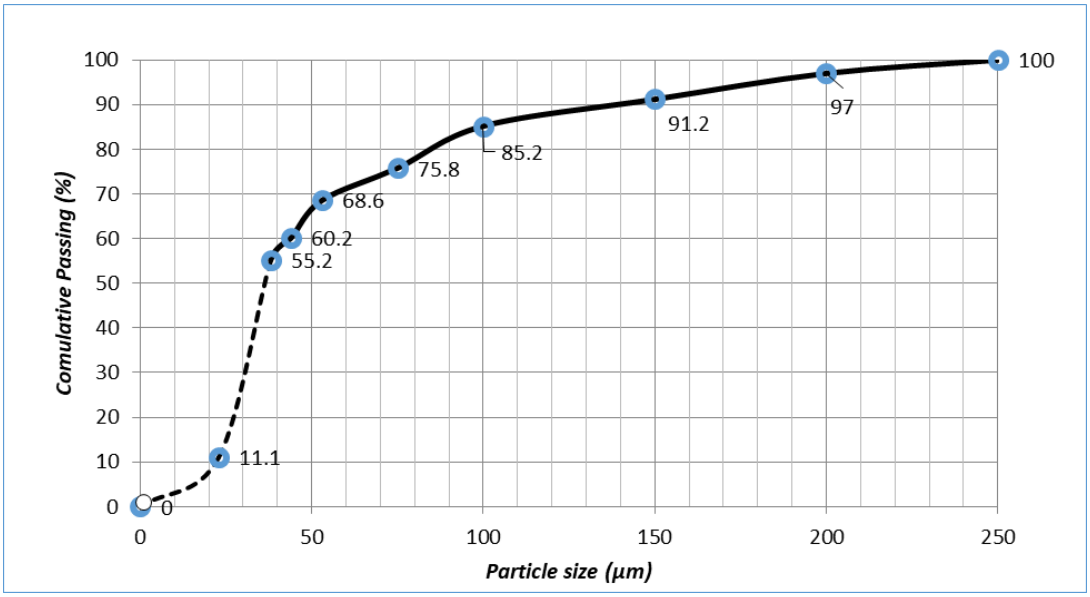

Figure 3. Particle size distribution for transported tailing to the tailing dam.

As shown in this figure, the particle size distribution indicates the values of d_{50} = 35 mic, d_{80} = 85, and d_{100} = 250 mic. Moreover, the solid density and the tailing pulp flow rate are measured as 2900 kg/m^3 and 18 t/h, respectively. The pulp properties such as the density and viscosity have been measured experimentally. The former is obtained by measuring the mass of a specific volume of pulp. The latter is calculated from the flow rate and elevation measurements. The properties of the pulp can also be calculated by simple mixture correlations, as follows:

$$\rho = S\rho_w \quad (32)$$

$$S = \frac{S_s}{S_s - C_w(S_s - 1)} \quad (33)$$

where the indices s and w refer to solid and water, respectively, C_w is the concentration of solid by weight, and S is the specific weight. The viscosity of pulp is a function of concentration. For most slurries, a particle volume fraction of 40% can be easily handled in a conventional piping system. However, viscosity increases drastically at higher concentrations [6]. Thus especial pumps are required to compensate for the resulting extremely high pressure drop. The following viscosity correlations are developed for the mixtures containing uniform size particles [44].

$$\mu = \mu_w[1 + 25C_v + 10.05{C_v}^2 + 0.00273\exp(16.6C_v)] \quad (34)$$

$$\mu = \mu_w[1 + \frac{3C_v}{1 - 1.923C_v}] \quad (35)$$

The viscosity can also be calculated from the well-known Einstein equation, as:

$$\mu = \mu_w(1 + 2.5c_v) \quad (36)$$

It should be noted that the effect of the particles agglomeration is neglected in Eqs. 34 and 36. Thus the measured viscosity values are expected to differ significantly from those obtained by the correlations.

6. Results

6.1. Validation of the experimental procedure

The primary experiments are carried out using water in order to investigate the accuracy of the measurements. The experimental data for variation of the flow rate with the water column elevation along with the theoretical results obtained from Eq. 13 is depicted in Figure 4 for two different cases. In case (a), the pipe inner diameter, length, and tank diameter are selected as d = 4.37 mm, L = 4 m, and with D = 81 mm. These parameters are changed to d = 7.18 mm, L = 6 m, and D =275 mm in the case (b).

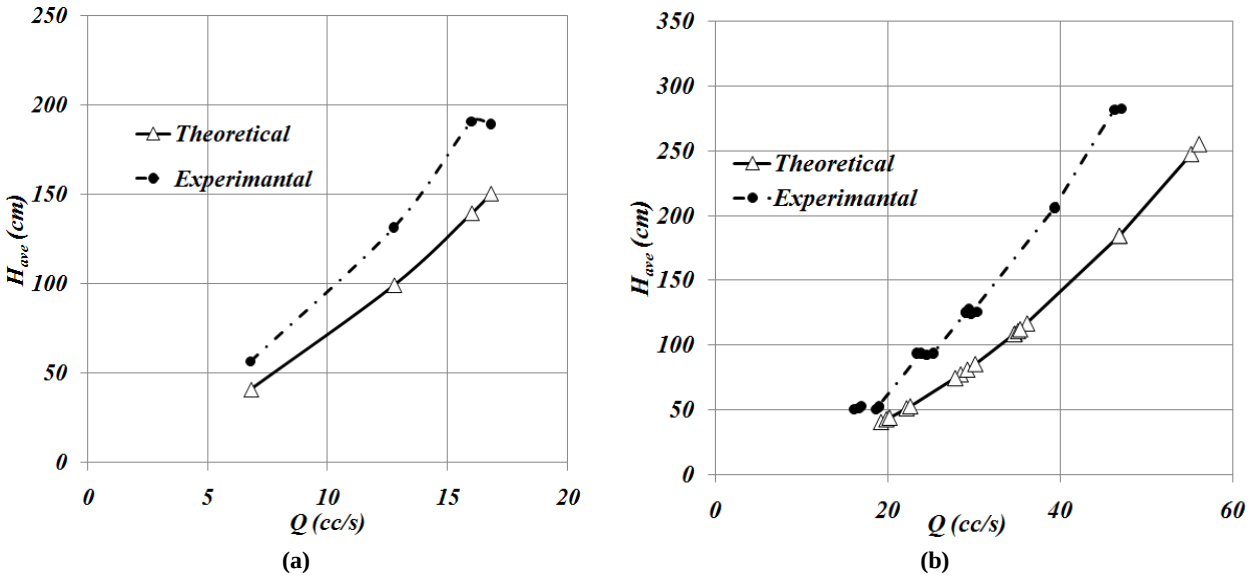

Figure 4. Comparison between the experimental and theoretical H-Q curves of water for (a) d = 4.37 mm, L = 4 m, and with D = 81 mm and (b) d = 7.18 mm, L = 6 m, and D = 275 mm.

As shown in this figure, there is a reasonable agreement between the theoretical and experimental values. The overall analysis of the data reveals that the turbulent and laminar flow assumptions fail in the ranges of Re < 2000 and Re > 4000, respectively. Moreover, it is not recommended to perform the experiments in the transition region of 2000 < Re < 4000. The inlet and exit losses can be neglected in the laminar flow, while they are significant in the turbulent regime. Furthermore, the transient flow effects must be considered for turbulent flows if the tank is small.

6.2. Comparison between pulp slurry and water curves

A comparison between the pulp and water flows is carried out in terms of the H-Q curve. The solid concentration by weight, C_w, in the pulp is 50%. Figs. 5 and 6 show the H-Q curves obtained for water and pulp for two different pipe sizes.

As shown in Figs. 5 and 6, the curves obtained for pulp and water consist of linear and non-linear parts corresponding to the laminar and turbulent regimes, respectively. For a constant flow rate, a higher H is required for pulp compared to water. This indicates a higher viscosity of the pulp. It can also be seen that the curves approach each other as the flow rate is increased. This implies that the apparent viscosity of the pulp decreases with increase in the flow rate. It is worth mentioning that the pulp curve does not pass through the origin. This can be attributed to the different rheology of the fluid, which is discussed in the following. Briefly, the pulp is a plastic fluid that requires a minimum shear stress to flow. This behavior can be attributed to the existence of extremely fine adhesive particles as well as clay in the pulp.

6.3. Main tests

The main tests are performed using the pulp samples with different specific gravities of S = 1.4, 1.5, 1.6, 1.65, 1.7, 1.75, 1.76. Moreover, the pipes with different lengths, L = 2.5, 5.8, 6 m, and diameters d = 7.06, 11.8 mm, are used in order to

achieve an extensive Reynolds number range. The tank size is kept constant with diameter of D = 81.5 mm. The initial and final pulp surface levels in the tank at a specific time interval as well as the pulp flow rate are measured during the experiments. These data is then used to calculate the shear stress and deformation rate. Table 1 summarizes the data obtained for the pulp flow with density of ρ=1400kg/m^3in a pipe with L = 5.8 m and d = 7.06 mm. The tank diameter is D = 81.5 mm.

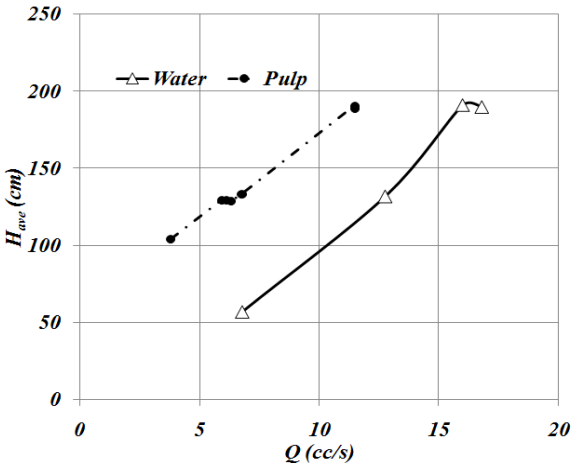

Figure 5. H-Q curves for water and pulp with Cw = 50% for pipe of d = 4.37 mm and L = 4 m and tank with D = 81 mm.

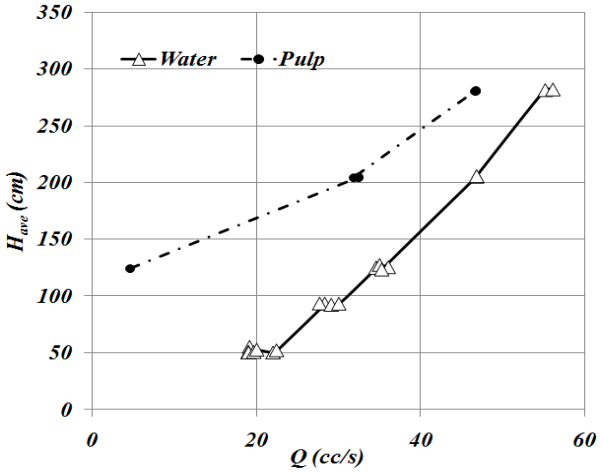

Figure 6. H-Q curves for water and pulp with Cw = 50% for pipe of d = 7.18 mm and L = 6 m and tank with D = 275 mm.

Table 1. Data obtained for pulp flow with density of $\rho = \frac{1400kg}{m^3}$ in a pipe with L = 5.8 m and d = 7.06 mm.

H_1 (cm)	H_2 (cm)	H_3 (cm)	V (cc)	t (s)	H_{ave} (cm)	Q (cc/s)	V_{ave} (m/s)
103	101.4	0	84.3	60	102	1.405	0.036
94	89.78	0	220	60	91.9	3.667	0.094
94	89.28	0	246.4	60	91.6	4.107	0.105
108	98.55	0	492.8	35	103	14.08	0.36
119	114.8	0	218.6	15	117	14.57	0.372
119	112.5	0	339	20	116	16.95	0.433
119	110.7	0	434	25	115	17.36	0.444
132.5	124.2	0	435.4	25	128	17.41	0.445
128	121.1	0	359.3	20	125	17.97	0.459
119	111.9	0	370	20	115	18.5	0.473
132.5	123.4	0	476	24	128	19.83	0.507
132.5	123	0	497	25	128	19.88	0.508
132.5	124.7	0	407	20	129	20.35	0.52
133	124.8	0	427.8	20	129	21.39	0.547
132.5	124.3	0	427.8	20	128	21.39	0.547
155	147.5	0	389.3	15	151	25.95	0.663
192	179	0	678	20	186	33.9	0.866
217	206.1	0	568	15	212	37.87	0.968
132.5	120.6	0	619.3	35	127	17.69	0.452
132.5	123	0	496	25	128	19.84	0.507
132.5	123	0	496	25	128	19.84	0.507
132.5	122.9	0	500	25	128	20	0.511
132.5	122.8	0	506	25	128	20.24	0.517
132.5	120.3	0	638.6	30	126	21.29	0.544

The pipe surface shear stress is calculated from Eqs. 15 and 16 for the data of Table 1. Figure 7 depicts the variation of the shear stress with deformation rate for the pulp density of S = 1.4.

Similarly, variation of the shear stress with deformation rate has been calculated for different pulp densities, and the results obtained are illustrated in Figure 8.

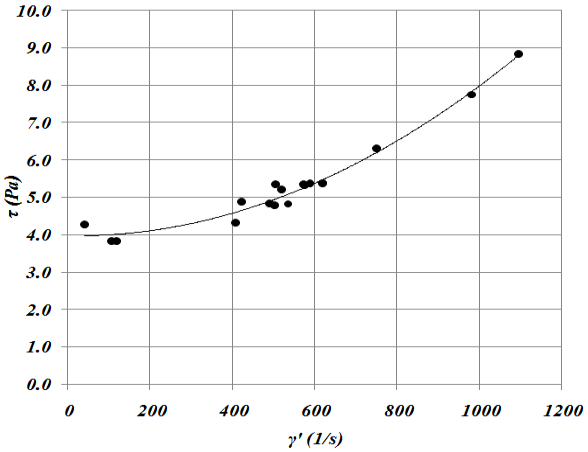

Figure 7. Variation in the shear stress with deformation rate for pulp density of S = 1.4.

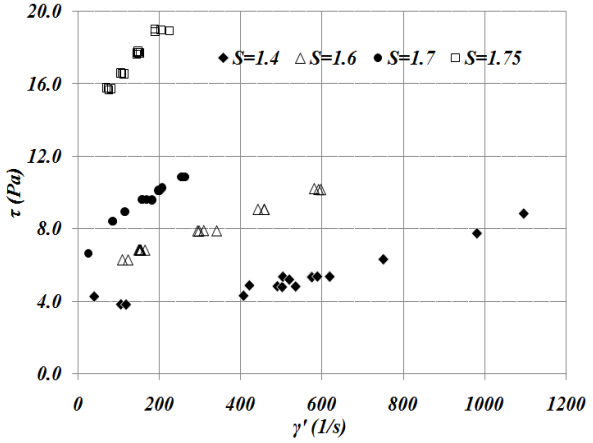

Figure 8. Variation in the shear stress with deformation rate for different pulp densities.

As shown in this figure, the shear stress increases with the velocity of the slurry flow. It is also shown that the curves do not pass through the origin, which means that the pulp exhibits a non-Newtonian behavior. Moreover, the pulp departs further from the Newtonian behavior as the density increases. In other words, it can be inferred that the yield stress and viscosity of pulp increase as the density increases, as expected. This increase is more significant at values higher than S = 1.6 (C_w = 63%).

6.4. Simulation of pulp behavior and development of correlation

The pulp flow behavior depends on several parameters such as the size and granular grading, concentration of solid particles in liquid, flow passage geometry, turbulent intensity, and viscosity of the carrier liquid (water). The dilute pulp containing large particles can generally be considered as a Newtonian fluid with the shear stress being a linear function of the deformation. This type of pulp sediment, and its viscosity is slightly greater than that of water at the low volume fractions ($C_v < 10\%$). The viscosity can be calculated from Eqs. 34-36. As the volume fraction of the particles increases, the particles get closer to each other and their contribution to the internal momentum transfer will dominate that of the base fluid. For the colloidal micro-sized particles, the fluid deviates from the Newtonian behavior, and exhibits a non-Newtonian behavior. Simulation of the non-Newtonian fluids is more difficult than the Newtonian ones. The shear stress is related to the deformation rate according to Eq. 21. In order to simulate the pulp with the plastic Bingham model, the values of the yield stress τ_0 and the apparent viscosity η must be obtained according to the method described in Section 4.2.1. The shear stress is obtained as a function of the deformation rate for all the slurry densities following the mentioned procedure, and the results obtained are illustrated in Figure 9.

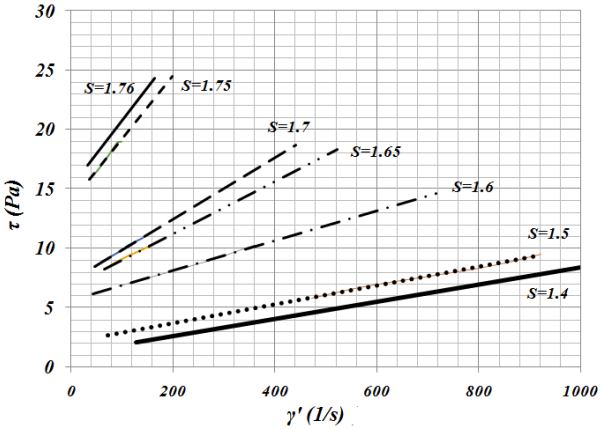

Figure 9. Variation in the shear stress with deformation rate for different pulp densities.

Having calculated the deformation rate for different pulp densities, the linear variations of the shear stress with the deformation rate are obtained, and the results obtained are summarized in Table 2.

Table 2. Bingham plastic model for pulps with different specific gravities.

Specific gravity	Shear stress
$S = 14$	$\tau = 0.73 + 7.1\dot{\gamma}$
$S = 1.5$	$\tau = 1.27 + 7.71\dot{\gamma}$
$S = 1.6$	$\tau = 4.19 + 7.73\dot{\gamma}$
$S = 1.65$	$\tau = 5.08 + 13.2\dot{\gamma}$
$S = 1.7$	$\tau = 5.49 + 13.8\dot{\gamma}$
$S = 1.75$	$\tau = 10.0 + 30.0\dot{\gamma}$
$S = 1.76$	$\tau = 10.4 + 39.4\dot{\gamma}$

The constant value in the right hand side of the shear stress in Table 2 is the yield stress, and the coefficient of the deformation rate is the apparent viscosity. Table 2 indicates that these parameters depend on the slurry density or equivalently the particle volume concentration.

The yield stress and the apparent viscosity have been correlated as functions of the volume concentration, as follows:

$$\tau_o = 0.035\exp(0.146c_v) \quad (37)$$

$$\eta = 6.3 + \frac{410}{(43.5 - c_v)^2} \quad (38)$$

6.5. Pipe selection

Three standard pipe sizes of 2.5 in, 3 in, and 4 in can be used for slurry transport in the Kooshk mine. The critical velocity and head lose have been calculated for these pipe sizes, as follows:

6.5.1. Critical velocity

The critical velocities are calculated from different correlations as a function of pipe diameters and particle concentrations, and the results obtained are summarized in Table 3.

Table 3. Critical velocities calculated from different correlations as a function of pipe diameter and particle concentration (Cw: concentration of solid by weight, Cv: concentration of solid by volume, Vc: critical velocity).

D(in)	Cw (%)	Ss	S	Cv (%)	Vc (m/s) DURAND	MOD. DURAND	CAVE	WASP	SCHILLER
2.00	50.00	2.90	1.49	25.64	1.11	1.18	0.67	0.99	0.33
2.00	60.00	2.90	1.65	34.09	1.11	1.18	0.67	1.05	0.34
2.00	70.00	2.90	1.85	44.59	1.11	1.18	0.66	1.10	0.35
2.5	50.00	2.90	1.49	25.64	1.21	1.23	0.71	1.05	0.36
2.5	60.00	2.90	1.65	34.09	1.21	1.23	0.71	1.11	0.37
2.5	70.00	2.90	1.85	44.59	1.21	1.23	0.70	1.17	0.38
3.00	50.00	2.90	1.49	25.64	1.32	1.29	0.75	1.12	0.39
3.00	60.00	2.90	1.65	34.09	1.32	1.29	0.75	1.18	0.40
3.00	70.00	2.90	1.85	44.59	1.32	1.29	0.74	1.24	0.42
4.00	50.00	2.90	1.49	25.64	1.46	1.35	0.80	1.20	0.43
4.00	60.00	2.90	1.65	34.09	1.46	1.35	0.79	1.26	0.45
4.00	70.00	2.90	1.85	44.59	1.46	1.35	0.79	1.33	0.46

Table 3 shows that different values are obtained using various correlations. It can be concluded that the slurry velocity is required to exceed 1 m/s to avoid sedimentation.

6.5.2. Head loss calculation

Pipe selection is based on the pressure drop calculation. The pressure drop is calculated for three different pipe sizes. The results obtained for three diameters of 2.5 in, 3 in, and 4 in are summarized in Tables 4, 5, and 6, respectively. The third and fourth columns are the yield stress and the apparent viscosity of the slurry. The fifth column indicates the required flow rate for transportation of the pulp with different concentrations. The Hedstrom, critical Reynolds and Reynolds numbers, and the resulting friction factors are also indicated in the tables. Finally, the head loss, H, and initiation head loss, H_s, are also calculated for two points, start of the tailing dam at the distance of 725 m and end of the tailing dam at 1450 m.

Table 4. Head loss calculation for a 2.5in pipe.

ρ (kg/m^3)	C_v (%)	τ_0 Pa	η Cp	Q_r L/s	He	Recr	Re	f	Pool inlet H (m)	Pool inlet Hs (m)	Pool outlet H (m)	Pool outlet Hs (m)
1300	16	0.4	6.8	10.9	41272	4993	40690	0.015	93	1	186	2
1350	18	0.5	7.0	9.4	60820	5982	35604	0.017	75	2	149	3
1400	21	0.8	7.1	8.2	88454	6669	31573	0.018	61	2	123	5
1450	24	1.1	7.3	7.3	126219	7360	28155	0.019	51	3	102	7
1500	26	1.6	7.7	6.6	174951	8247	25039	0.019	43	5	86	10
1550	29	2.4	8.2	6.0	231346	9155	21958	0.02	37	7	75	14
1600	32	3.5	9.2	5.5	281953	9787	18630	0.023	35	10	70	20
1650	34	5.2	11.1	5.0	294950	9966	14740	0.029	38	14	76	28
1700	37	7.6	15.5	4.7	225407	9035	10022	0.043	49	20	98	41
1750	39	11.1	31.6	4.4	82549	6360	4740	0.072	71	29	141	58
1800	42	16.4	217.1	4.1	2641	2456	665	0.183	159	41	317	83

Table 5. Head loss calculation for a 3 in pipe.

ρ (kg/m^3)	C_v (%)	τ_0 Pa	η Cp	Q_r L/s	He	Recr	Re	f	Pool inlet H (m)	Pool inlet Hs (m)	Pool outlet (kg/m^3)	Pool outlet (%)
1300	16	0.4	6.8	10.9	62519	5836	33060	0.017	37	1	73	2
1350	18	0.5	7.0	9.4	92130	6759	28928	0.018	29	1	58	3
1400	21	0.8	7.1	8.2	133990	7547	25653	0.019	23	2	47	4
1450	24	1.1	7.3	7.3	191196	8581	22876	0.02	19	3	39	6
1500	26	1.6	7.7	6.6	265014	9573	20344	0.021	17	4	33	8
1550	29	2.4	8.2	6.0	350441	10020	17841	0.025	16	6	33	11
1600	32	3.5	9.2	5.5	427101	11357	15137	0.036	20	8	39	16
1650	34	5.2	11.1	5.0	446788	11534	11976	0.057	26	12	53	23
1700	37	7.6	15.5	4.7	341445	10479	8143	0.091	37	16	73	33
1750	39	11.1	31.6	4.4	125044	7376	3851	0.149	52	24	104	47
1800	42	16.4	217.1	4.1	4000	2668	540	0.317	97	34	194	67

Table 6. Head loss calculation for a 4 in pipe.

ρ (kg/m^3)	C_v %	τ_0 Pa	η Cp	Q_r L/s	He	Recr	Re	f	Pool inlet H (m)	Pool inlet Hs (m)	Pool outlet (kg/m^3)	Pool outlet (%)
1300	16	0.4	6.8	10.9	88162	6468	27840	0.018	17	1	34	2
1350	18	0.5	7.0	9.4	129918	7489	24361	0.019	13	1	26	2
1400	21	0.8	7.1	8.2	188947	8480	21602	0.02	10	2	21	3
1450	24	1.1	7.3	7.3	269616	9611	19264	0.022	9	2	18	5
1500	26	1.6	7.7	6.6	373711	10839	17132	0.027	9	3	18	7
1550	29	2.4	8.2	6.0	494176	12012	15024	0.041	11	5	23	10
1600	32	3.5	9.2	5.5	602279	12924	12747	0.066	15	7	31	14
1650	34	5.2	11.1	5.0	630040	13092	10085	0.108	21	10	42	19
1700	37	7.6	15.5	4.7	481491	11882	6857	0.174	30	14	59	28
1750	39	11.1	31.6	4.4	176332	8312	3243	0.281	42	20	83	40
1800	42	16.4	217.1	4.1	5641	2979	455	0.532	69	28	138	57

In Tables 4, 5, and 6, the cases for which the pipe flow cannot be established by the elevation head (geometrical height difference) and a pumping system is required are determined and highlighted. For example, using a 2.5 in pipe will necessitate application of a pump for all the volume fractions because of the friction head losses that might occur, while delivering the slurry to the inlet and exit of the dam are more than 29 m and 44 m, respectively. Although a 2.5 pipe has a lower cost than 3 in pipe, its usage is noted beneficial considering the pump cost and power consumption. A 4 in pipe can be used without pump for transportation of pulp with solid volume fractions lower than C_v = 34%. However, it should be noted that the flow velocity might decrease below the critical value required to avoid sedimentation. Using 4 in pipes will cause a 50% increase in the cost of piping system compared to that of 3 in pipes. Limitations of the 3 in pipe for concentrations higher than C_v = 34% are similar to those of the 4 in pipes. In addition, using a pump is inevitable for concentrations lower than C_v = 24%. Therefore, it can be concluded that a 3 in pipe is a suitable selection for the pulp with concentrations of $20 < C_v < 35$. This piping system can be used without the application of a pump.

Based on the above discussion, the appropriate piping system that can deliver the slurry has been determined and illustrated in Figure 10.

Location of the pipe is shown by points A, E, F, G, and H. The heights and distances of the points are shown in Table 7.

Table 7. Heights and distances of different points on the piping system.

Height, H (m)	Length, L (m)	Point
30	750	E
35	940	F
46	1160	G
56	1350	H

Figure 10 shows the operational conditions at the different locations of the piping system for different slurry concentrations.

ρ	Cw	Cv	Taw0	eta	Q	He	f(fi)	fi	Recr	a	k	v	Re	fl	ft	m	f	E		F		G		H	
kg/m3	%	%	Pa	Cp	L/s							m/s						H(m)	Hs(m)	H(m)	Hs(m)	H(m)	Hs(m)	H(m)	Hs(m)
1300	35	16	0.4	6.8	10.9	62519	3.72	0.49	5805	-1.51	0.13	2.17	33060	0.003	0.017	2.91	0.017	38	1	48	1	59	2	68	2
1320	37	17	0.4	6.9	10.2	73104	4.35	0.51	6105	-1.50	0.13	2.04	31274	0.003	0.017	2.98	0.017	34	1	43	1	53	2	62	2
1340	39	18	0.5	6.9	9.6	85334	5.08	0.53	6433	-1.49	0.13	1.92	29672	0.004	0.018	3.05	0.018	31	1	39	2	49	2	56	2
1360	40	19	0.6	7.0	9.1	99416	5.92	0.55	6790	-1.48	0.13	1.81	28218	0.004	0.018	3.12	0.018	29	2	36	2	44	2	52	3
1380	42	20	0.6	7.0	8.6	115564	6.88	0.57	7176	-1.48	0.13	1.72	26886	0.005	0.019	3.19	0.019	26	2	33	2	41	3	47	3
1400	44	21	0.8	7.1	8.2	133990	7.98	0.58	7547	-1.47	0.13	1.63	25653	0.006	0.019	3.26	0.019	24	2	30	3	37	3	43	4
1420	45	22	0.9	7.2	7.8	154888	9.22	0.60	7942	-1.47	0.13	1.55	24498	0.007	0.019	3.33	0.019	22	2	28	3	34	4	40	4
1440	47	23	1.0	7.3	7.4	178415	10.62	0.61	8359	-1.47	0.14	1.48	23404	0.008	0.019	3.41	0.020	21	3	26	3	32	4	37	5
1460	48	24	1.2	7.4	7.1	204659	12.18	0.63	8739	-1.47	0.14	1.42	22357	0.010	0.020	3.49	0.020	19	3	24	4	30	5	35	6
1480	50	25	1.4	7.5	6.8	233593	13.90	0.64	9185	-1.47	0.14	1.36	21341	0.012	0.020	3.57	0.021	18	4	23	5	28	6	33	7
1500	51	26	1.6	7.7	6.6	265014	15.77	0.65	9573	-1.47	0.14	1.30	20344	0.014	0.020	3.67	0.021	17	4	22	5	27	6	31	7
1520	52	27	1.9	7.9	6.3	298456	17.77	0.67	9983	-1.47	0.14	1.25	19352	0.017	0.020	3.77	0.022	17	5	21	6	26	7	30	9
1540	54	28	2.2	8.1	6.1	333081	19.83	0.68	10366	-1.47	0.14	1.21	18350	0.020	0.020	3.88	0.024	17	6	21	7	26	9	30	10
1560	55	29	2.6	8.4	5.8	367543	21.88	0.69	10737	-1.47	0.14	1.16	17324	0.024	0.021	4.01	0.027	17	6	22	8	27	10	31	11
1580	56	31	3.0	8.7	5.6	399828	23.80	0.69	11067	-1.47	0.14	1.12	16259	0.029	0.021	4.16	0.031	19	7	23	9	29	11	33	13
1600	57	32	3.5	9.2	5.5	427101	25.42	0.70	11357	-1.47	0.14	1.09	15137	0.035	0.021	4.34	0.036	20	8	26	11	31	13	37	15
1620	58	33	4.1	9.8	5.3	445613	26.52	0.70	11503	-1.47	0.14	1.05	13943	0.043	0.021	4.57	0.043	23	10	28	12	35	15	41	17
1640	60	34	4.8	10.6	5.1	450778	26.83	0.70	11550	-1.47	0.14	1.02	12658	0.052	0.022	4.86	0.052	26	11	32	14	40	17	46	20
1660	61	35	5.6	11.6	5.0	437604	26.05	0.70	11465	-1.47	0.14	0.99	11267	0.062	0.022	5.25	0.062	29	13	36	16	45	20	52	23
1680	62	36	6.5	13.2	4.8	401750	23.91	0.69	11080	-1.47	0.14	0.96	9761	0.075	0.023	5.80	0.075	33	15	42	19	51	23	60	27
1700	63	37	7.6	15.5	4.7	341445	20.32	0.68	10479	-1.47	0.14	0.93	8143	0.091	0.024	6.61	0.091	38	17	47	21	59	26	68	31
1720	64	38	8.8	19.3	4.5	260154	15.49	0.65	9523	-1.47	0.14	0.91	6437	0.111	0.025	7.91	0.111	43	20	54	25	67	30	78	35
1740	65	39	10.3	26.1	4.4	168915	10.05	0.61	8207	-1.47	0.14	0.88	4700	0.135	0.026	10.21	0.135	50	23	63	28	77	35	90	41
1760	66	40	12.0	39.8	4.3	85692	5.10	0.53	6460	-1.49	0.13	0.86	3036	0.166	0.028	14.88	0.166	58	26	73	33	90	40	105	47
1780	67	41	14.0	74.8	4.2	28605	1.70	0.39	4518	-1.56	0.11	0.84	1592	0.211	0.026	26.83	0.211	70	30	88	38	109	47	127	54
1800	68	42	16.4	217.1	4.1	4000	0.24	0.15	2668	-1.66	0.09	0.81	540	0.317	0.026	75.71	0.317	100	35	126	44	155	54	181	63

Figure 10. Operational conditions for slurry transport to the different locations of the piping system.

The required pumping head to deliver the slurry to point H as a function of the slurry flow rate and density is depicted in Figure 11.

As shown in Figure 12, the required head increases with the slurry density. However, the head increase is more significant at lower flow rates.

Variation in the friction coefficient with the Reynolds number is plotted in Figure 12 for different slurry densities.

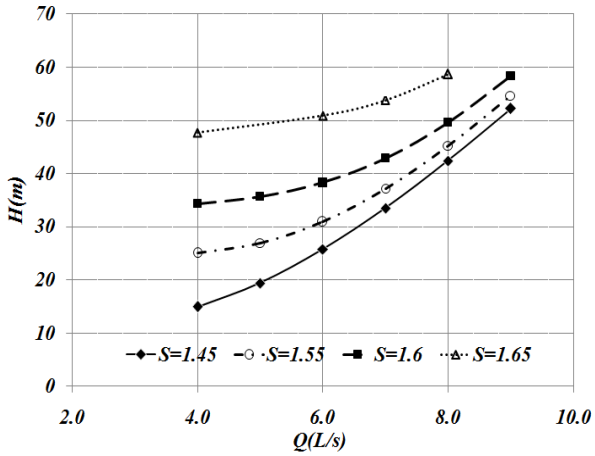

Figure 11. Required pumping head to deliver the slurry to point H (Table 7) as a function of the slurry flow rate and density.

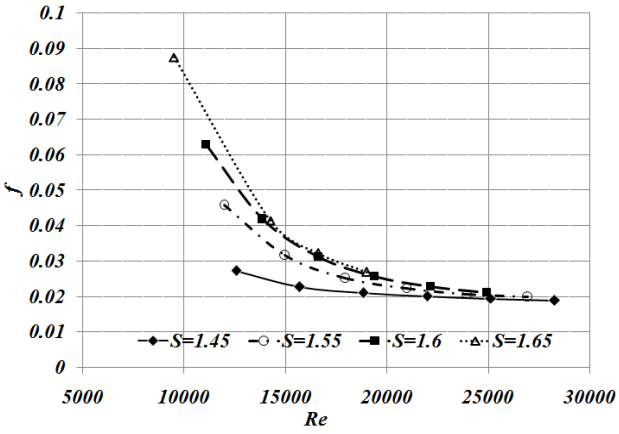

Figure 12. Variation in the friction coefficient with Reynolds number for different slurry densities.

As shown in this figure, the friction factor changes drastically with the Reynolds number at higher specific gravities, while the effect Reynolds number is not significant at lower densities.

7. Economical evaluation of piping system.

A comparison between the current open channel and designed piping system from the viewpoint of water consumption is presented in Table 9. Slurry transport to the tailing dam with the current open channel in the Kooshk mine is performed with an average solid concentration of 40% by weight, and it is accompanied with a considerable water loss of 1.5 m^3 per ton of dry solid material. Replacement of the open channel with the designed piping system allows the transportation of slurry of 55%

concentration with the water loss reduced to 0.8 m^3 per ton of dry solid material. The resulting water saving of 45.5% will exceed 5113.6 m^3 water per month. In addition, using the proposed piping system, the number of unplanned shut downs of the processing plant will be reduced, which, in turn, will cause 45 tons further production Zn concentrate per month, as indicated in Table 10. This production improvement is equivalent to 42750 $/month, and the net profit of 21375 $/month is expected.

Table 9. Comparison of water consumption in the open channel and designed pipe system.

Transport system	Solid percent (%)	Water loss (m^3/ton)	Water (saving %)	Water loss to tailing dam (m^3/day)	Water recycle from tailing dam (m^3/day)	Water Consumption (m^3/month)	Water saving (m^3/month)
Open channel	40	1.5		600	150	11250	
Designed piping system	55	0.8	45.5	327.3	81.8	6136.4	5113.6

Table 10. Concentrate production.

Concentrate production t/day	Zn concentrate value ($/t)	Concentrate value ($/month)	Profit/month
45	950	42750	21375

The proposed piping system will require an additional cost for the pipes and other related equipment. The total costs for the piping system investment are summarized in Table 11.

Table 11. Piping system investment cost.

Item	Cost
Pipe 3 in	9000
Engineering and consultant	5000
valves	1500
Thickener underflow control system (magnetite flowmeter Pinch valve + densitometer, etc.)	30000
Thickener underflow discharge tank	1000
Installation	3000
Unpredicted	5000
Total	**54500**

Evaluation of Tables 9-11 reveals that the piping system investment will be paid back in 3 months.

8. Conclusions

An experimental study was carried out to design a piping system for the slurry transport to the tailing dam in the Kooshk lead-zinc mine in Iran. The design process consisted of several steps. Primarily, the particle type, size, and density were determined, and the pulp slurry density was measured. Then the experiments were conducted to investigate the rheological behavior of the slurry at different densities, and obtain a non-Newtonian model for the shear stress variation with the deformation rate. The results obtained indicate that the shear stress of concentrated slurry exhibits a similar behavior to the plastic Bingham model. The yield stress and the apparent viscosity of the slurry were calculated for different conditions. These parameters were shown to have direct relations with the density. Appropriate correlations were also proposed for the apparent viscosity and yield stress of the slurry as a function of particle concentration. Using the developed correlations, the slurry flow rate, pressure drop, critical velocity, minimum head for flow initiation, and head losses were calculated for different slurry densities and pipe sizes. Finally, the 3 in diameter pipe was selected to be used to deliver the slurry percent solids between 44% < C_w < 60% to the desired location. The selected piping system could operate without the application of a pumping system. However, controlling the slurry concentration was key a parameter, which was required to be adjusted precisely. Another important point worth mentioning is that water can be saved by 45.5% for the slurry transport using the proposed piping system. In addition, the unplanned shut down of the processing plant will be decreased, which directly impacts on the plant annual concrete production rate.

Acknowledgments

The authors are very grateful to Mr. Ali Reza Entezari for his guidance in this work. In addition, the authors would like to thank the “Bafgh Mine Company” and the “Iranian Deputy Ministry of Mining and Mineral Industries Affairs” for their financial supports.

References

[1]. Fangary, Y.S., Ghani, A.A., El Haggar, S.M., and Williams, R.A. (1997). The effect of fine particles on slurry transport processes. Minerals engineering. 10 (4): 427-439.

[2]. Islam, S., Williams, D.J., Llano-Serna, M., and Zhang, C. (2020). Settling, consolidation, and shear strength behaviour of coal tailings slurry. International Journal of Mining Science and Technology. 30 (6): 849-857.

[3]. Wasp, E.J., Kenny, J.P., and Gandhi, R.L. (1979). Solid-liquid flow slurry pipeline transportation. Gulf Pub. Co.

[4]. Wilson, K.C., Addie, G.R., Sellgren, A., and Clift, R. (2006). Slurry transport using centrifugal pumps. Springer.

[5]. Dunne, R.C., Kawatra, C.A., Young, C.A. (2019). SME Mineral Processing and Extractive Metallurgy Handbook, Society for Mining, Metallurgy, and Exploration, 743 P.

[6]. McKetta Jr, J.J. (1992). Piping design handbook, CRC Press, 94 P.

[7]. Pinto, T.S., Junior, D.M., Slatter, P.T., and Leal Filho, L.S. (2014). Modelling the critical velocity for heterogeneous flow of mineral slurries. International journal of multiphase flow. 65: 31-37.

[8]. Durand, R. (1952). The Hydraulic Transportation of Coal and Other Materials in Pipes, Colloq, off National Coal Board, London.

[9]. Wilson, K.C. and Addie, G.R. (1997). Coarse-particle pipeline transport: effect of particle degradation on friction. Powder technology. 94 (3): 235-238.

[10]. Thomas, A.D. (1979). Predicting the deposit velocity for horizontal turbulent pipe flow of slurries. International Journal of Multiphase Flow. 5 (2): 113-129.

[11]. Wasp, E.J. and Slatter, P.T. (2004). Deposition velocities for small particles in large pipes, In international conference on transport and sedimentation of solids particles, 12th, Prague: Institute of Hydrodynamics, Academy of Sciences of the Czech Republic, 20-24.

[12]. Doron, P. and Barnea, D. (1993). A three-layer model for solid-liquid flow in horizontal pipes. International Journal of Multiphase Flow. 19 (6): 1029-1043.

[13]. Lahiri, S.K. and Ghanta, K.C. (2008). Prediction of pressure drop of slurry flow in pipeline by hybrid support vector regression and genetic algorithm model. Chinese Journal of Chemical Engineering. 16 (6): 841-848.

[14]. Gillies, D., Sanders, R.S., and Gillies, R.G. (2010). Determining the maximum coarse particle concentration for slurry pipeline flow, Hydrotransport 18th, Rio de Janeiro, BHR Group, 105-115.

[15]. Turian, R.M. and Yuan, T.F. (1977). Flow of slurries in pipelines. AIChE Journal. 23(3): 232-243.

[16]. Miedema, S.A. (2017). A new approach to determine the concentration distribution in slurry transport, Proceedings Dredging Summit and Expo, Western Dredging Association, Bonsall, CA, USA. 189-203.

[17]. Kaushal, D.R. and Tomita, Y. (2007). Experimental investigation for near-wall lift of coarser particles in slurry pipeline using γ-ray densitometer. Powder technology. 172 (3): 177-187.

[18]. Wilson, K.C. and Sellgren, A. (2003). Interaction of particles and near-wall lift in slurry pipelines. Journal of Hydraulic Engineering. 129 (1): 73-76.

[19]. Tarodiya, R. and Gandhi, B.K. (2020). Effect of particle size distribution on performance and particle kinetics in a centrifugal slurry pump handling multi-size particulate slurry. Advanced Powder Technology. 31 (12): 4751-4767.

[20]. Knezevic, D. and Kolonja, B. (2008). The influence of ash concentration on change of flow and pressure in slurry transportation. International Journal of Mining and Mineral Engineering. 1 (1): 104-112.

[21]. Wu, D., Yang, B., and Liu, Y. (2015). Pressure drop in loop pipe flow of fresh cemented coal gangue–fly ash slurry: Experiment and simulation. Advanced Powder Technology. 26 (3): 920-927.

[22]. Wang, X.M., Li, J.X., Xiao, Z.Z., and Xiao, W.G. (2004). Rheological properties of tailing paste slurry. Journal of Central South University of Technology. 11 (1): 75-79.

[23]. Wu, D., Fall, M., and Cai, S.J. (2013). Coupling temperature, cement hydration and rheological behaviour of fresh cemented paste backfill. Minerals Engineering. 42: 76-87.

[24]. Senapati, P.K. and Mishra, B.K. (2012). Design considerations for hydraulic backfilling with coal combustion products (CCPs) at high solids concentrations. Powder Technology. 229: 119–125.

[25]. Xiao, B., Fall, M., and Roshani, A. (2021). Towards Understanding the Rheological Properties of Slag-Cemented Paste Backfill. International Journal of Mining, Reclamation and Environment. 35 (4): 268-290.

[26]. Verma, A.K., Singh, S., and Seshadri, V. (2006). Effect of particle size distribution on rheological properties of fly ash slurries at high concentrations. International Journal of Fluid Mechanics Research. 33 (5).

[27]. Cao, S., Xue, G., Yilmaz, E., and Yin, Z. (2021). Assessment of rheological and sedimentation characteristics of fresh cemented tailings backfill slurry. International Journal of Mining, Reclamation and Environment. 35 (5): 319-335.

[28]. Miedema, S.A. (2015). A head loss model for slurry transport in the heterogeneous regime. Ocean

Engineering. 106: 360-370.

[29]. Wu, D., Yang, B., and Liu, Y. (2015). Transportability and pressure drop of fresh cemented coal gangue-fly ash backfill (CGFB) slurry in pipe loop, Powder Technology. 284: 218–224.

[30]. Kumar, N., Gopaliya, M.K., and Kaushal, D.R. (2016). Modeling for slurry pipeline flow having coarse particles. Multiphase Science and Technology. 28 (1):1-33.

[31]. Li, M. Z., He, Y.P., Liu, Y.D., and Huang, C. (2018). Hydrodynamic simulation of multi-sized high concentration slurry transport in pipelines. Ocean Engineering. 163: 691-705.

[32]. Ling, J., Skudarnov, P.V. Lin, C.X., and Ebadian, M.A. (2003). Numerical investigations of liquid-solid slurry flows in a fully developed turbulent flow region, Internal Journal Heat Fluid Flow. 24 (3): 389-398.

[33]. Li, M., He, Y., Jiang, R., Zhangc, J., Zhangd, H., Liu, W., and Liu,Y. (2021). Analysis of minimum specific energy consumption and optimal transport concentration of slurry pipeline transport systems, Particuology. In Press, doi: https://doi.org/10.1016/j.partic.2021.08.004.

[34]. Jati, H.A. Monei, N. Barakos, G., Tost, M., and Hitch, M. (2021). Coal slurry pipelines: A coal transportation method in Kalimantan, Indonesia, International Jpurnal of Mining, Reclamation and Environmrnt, https://doi.org/10.1080/17480930.2021.1949857.

[35]. Cunliffe, C.J., Dodds, J.M., and Dennis, D.J.C. (2021). Flow correlations and transport behaviour of turbulent slurries in partially filled pipes. Chemical Engineering Science. 235: 116465.

[36]. White, F.M. (1986). Fluid mechanics, 1st Ed., McGraw-Hill., New York.

[37]. Streeter, V.L., Willy, E.B., and Bedfard, K.W. (1998). Fluid mechanics, 3st Ed., McGraw-Hill.

[38]. Elvain, R. and Cave, I. (1972). Transportation of Tailings, World Mining Tailings Symposium.

[39]. Schiller, R.E. and Herbich, J.B. (1991). Sediment transport in pipes, McGraw-Hill., New York.

[40]. Hedstrm, B.O. (1952). Flow of plastic materials in pipes. Industrial and Engineering Chemistry. 44 (3): 651-656.

[41]. Darby, R. (1981). How to predict the friction factor for flow of Bingham plastics. Chemical engineering. 28: 59-61.

[42]. Hanks, R.W. (1967). On the flow of Bingham plastic slurries in pipes and between parallel plates. Society of Petroleum Engineers Journal. 7 (4): 342-346.

[43]. Darby, R., Mun, R., and Boger, D. (1992), Predict friction loss in slurry pipes, Chemical engineering. 99 (9):116–119.

[44]. Thomas, D.G. (1965). Transport characteristics of suspension: VIII, A note on the viscosity of Newtonian suspensions of uniform spherical particles. Journal of colloid science. 20 (3): 267-277.

مطالعه تجربی انتقال پالپ باطله معدن سرب و روی کوشک بر اساس رئولوژی سیال غیر نیوتنی

جواد وظیفه مهربانی[1*] و محمد گوهرخواه[2]

۱- دانشکده مهندسی معدن، دانشگاه صنعتی سهند، تبریز، ایران
۲- دانشکده مهندسی مکانیک، دانشگاه صنعتی سهند، تبریز، ایران

ارسال ۲۰۲۱/۰۸/۲۴، پذیرش ۲۰۲۱/۰۹/۲۵

* نویسنده مسئول مکاتبات: mehrabani@sut.ac.ir

چکیده:

در این کار تحقیقاتی، یک سیستم لوله‌کشی برای انتقال پالپ باطله معدن سرب و روی کوشک جهت انتقال به سد باطله طراحی شده است. در گام نخست، با انجام آزمایش‌هایی، رفتار پالپ در چگالی‌های مختلف مورد بررسی قرار گرفته و یک مدل غیر نیوتنی برای تغییرات تنش برشی سیال نسبت به نرخ تغییر شکل بدست آمد. بر اساس نتایج حاصل، تنش برشی پالپ با غلظت جامد بالا، از مدل پلاستیکی بینگهام پیروی می‌کند. نتایج به دست آمده همچنین بیانگر روند افزایشی تنش تسلیم و ویسکوزیته ظاهری پالپ با افزایش چگالی است. همبستگی مناسبی نیز بین ویسکوزیته ظاهری و تنش تسلیم نسبت به غلظت چامد پالپ مشاهده گردید. در مرحله بعد، پارامترهای طراحی مورد نیاز مانند: دبی پالپ ،افت فشار، سرعت بحرانی و حداقل فشار مورد نیاز جهت راه اندازی جریان پالپ در لوله، در چگالی‌ها و اندازه لوله‌های مختلف، محاسبه گردیدند. در نهایت، سیستم لوله‌کشی مناسب بر اساس داده‌های آزمایشگاهی و پارامترهای محاسبه شده، طراحی شد. براین اساس، لوله با قطر داخلی ۳ اینچ برای انتقال پالپ با درصد وزنی جامد بین ۴۰ تا ۶۰ درصد و بدون نیاز به سیستم پمپاژ، پیشنهاد گردید.

کلمات کلیدی: پالپ باطله، سرعت بحرانی، طراحی لوله، مدل بینگهام، معدن کوشک.